Praktikum Nanocharacterization I

Scanning Electron Microscopy

Contents:

- Use of SEM for imaging of different samples at different magnifications and different imaging modes
- Different contrast mechanisms
- Determine geometrical dimensions of various structures

Basic Functions and Working Principle

Scanning Electron Microscopy

1. Introduction

Electrons microscopes provide a very **high spatial resolution** down to ~ nm due to the orders of magnitude shorter wavelength of electron beams compared to visible light.

$$r_{diff} = 0.61 \cdot \lambda / n \sin\alpha$$

This drastically reduces the diffraction limit.

De Broglie wavelength of electrons:

$$\lambda_{electron} = \frac{h}{m v} = 1.225 nm / \sqrt{E(eV)}$$ (E < 100keV)

compare photon wavelength: $\lambda_{photon} = c / \upsilon = 1240\ nm / E\,[eV]$ (E ~ 1-3eV)

Relativistic electrons: $\lambda_{rel} = h / [2\, m_{0,e} \cdot E\,(1 + E/2\, m_{0,e} \cdot c^2)]^{1/2}$ (E > 100kV).

⇨ For electron energies E > 150 eV the electron wavelength is λ <1 Å !

This also applies to protons or ion beams where λ << 1 Å already for E >1eV.

Comparison of Accelerating Voltage, Wavelength, and Resolving Power for a Transmission Electron Microscope

As accelerating voltage increases, wavelength decreases and resolution decreases (improves).

ACCELERATING VOLTAGE (V)	WAVELENGTH (nm)	RESOLUTION (nm)
20,000	0.0087	0.44
40,000	0.0061	0.31
60,000	0.0050	0.25
80,000	0.0043	0.21
100,000	0.0039	0.19
1,000,000	0.00087	0.10

Scanning electron microscope – SEM: E ~ 2 – 50 keV,
Transmission electron microscope – TEM: E ~ 50 – 300 keV

2. Scanning Electron Microscopes

- In SEM, the sample is raster ***scanned*** with a sharply ***focused electron beam*** of a few nm diameter and energy of 5 - 50 keV. The ***magnification M*** is the ratio between **scan size /display size**.
- SEM images = Lateral intensity distribution of **backward *emitted secondary electrons*** or of the ***backscattered electrons*** recorded as a function of the beam position on the sample. Alternatively, the excited x-ray photons, luminescence or sample current images can be recorded.

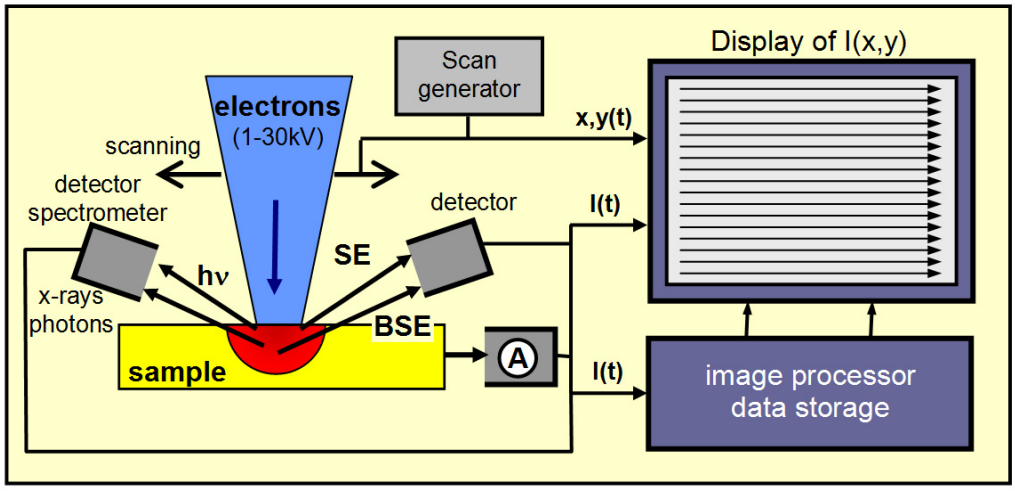

Features: High resolution (~few nm), no sample preparation needed, chemical analysis & spectroscopy

⇨ **Resolution** depends on probe size and interaction volume. Trend towards lower electron energies.

⇨ **Contrast** depends on the interaction mechanisms, beam parameters and detection schemes.

Instrumentation

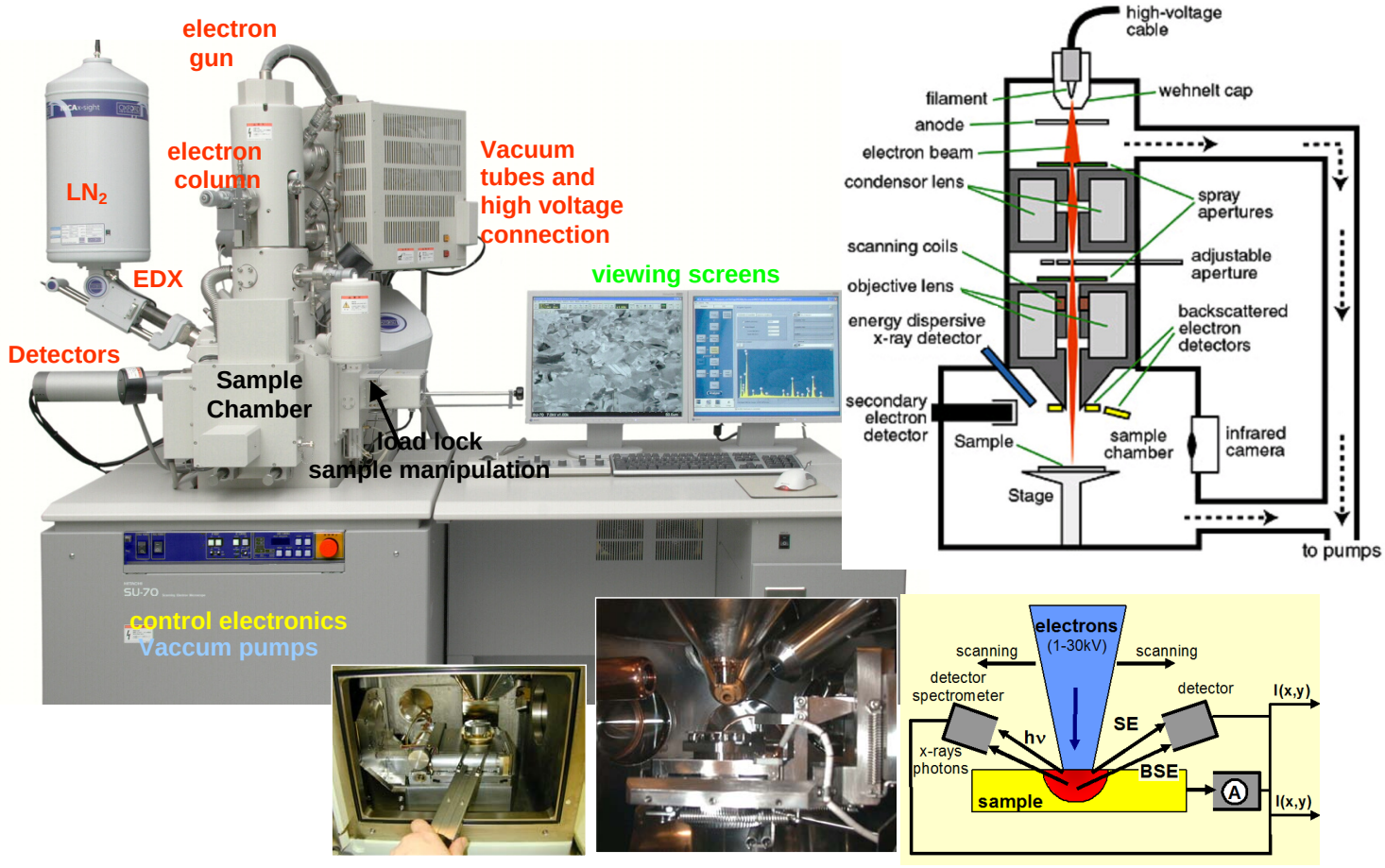

Basic Components

Electron microscopes consist of following components:

- **Electron source**: Electron gun and high voltage sources
- **Electro-optical column** with electron optics (magnetic or electrostatic lenses, beam deflection, apertures, ..)
- **Sample chamber** with movable and tiltable sample stage
- **Electron detectors** + optional x-ray detectors for chemical analysis
- **High vacuum system:** HV pumps, valves pressure gauges, …
- **Load lock chamber** for rapid sample exchange
- **Control electronics** & computer control system
- **Image analysis** and processing software
- **Sample preparation**:
  TEM: Thinning / cutting / polishing
  SEM: Conductive coating (Au, graphite , …)

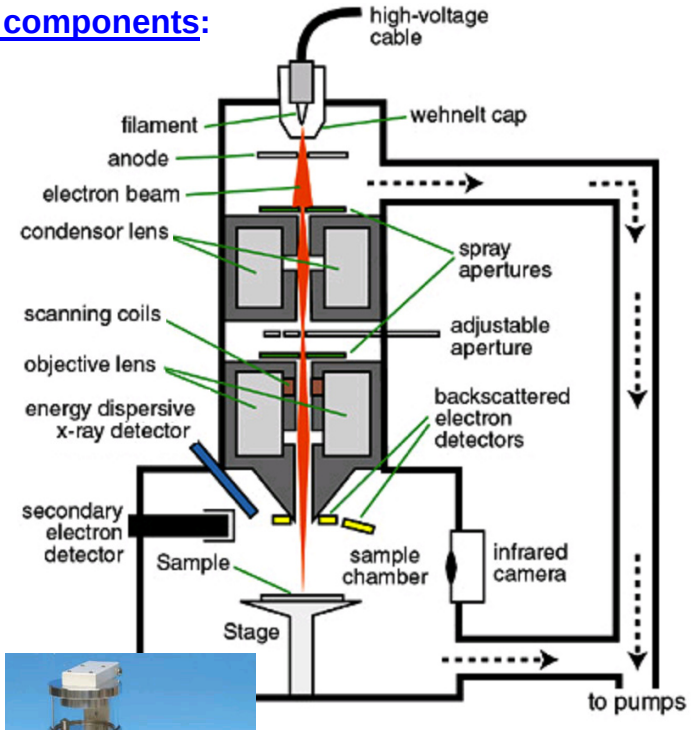

Electron Lenses

$r_{eff} = (r^2_{dif} + r^2_{aber})^{1/2}$

Because the aberrations of electron lenses are very larger, i.e., $r_{aber} > r_{diff}$ the *practical resolution* of electron microscopes is mostly limited by lens aberrations.

Electron Lenses

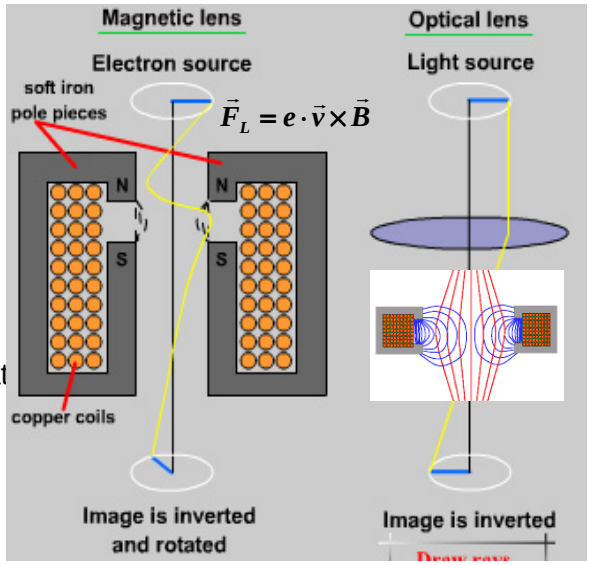

Electrons can be deflected by electric *or* magnetic fields, but **magnetic fields** are generally more effective at high electron energies because the Lorentz force increases with electron velocity.

For a focusing action, a **nonuniform radially varying B-field distribution** is required such that outer electrons are bend more strongly towards the optical axis than near-axis electrons.

Such a nonuniform magnetic field is produced by the stray field of a coil surrounded by a iron pole piece that is interrupted by a gap in the central bore.

Since the field strength can be changed through the applied voltage or current, the focal length of electron lenses can be continuously adjusted.

Aberrations: Due to the non-ideal magnetic field distribution, electron lenses exhibit very large intrinsic lens aberrations.

Due to these aberrations, the aperture angles of electron lenses must be kept very small, in order to limit the effect of lens errors, which rapidly increases with α^n . Typically $\alpha \leq 0.3°$!

⇒ Achievable NA is much smaller than for optical lenses: $NA_{TEM} \sim 0.005 \Rightarrow r_{eff} \sim 100\ \lambda$

Principle of Magnetic Electron Lenses

Magnetic lenses consist of a *coil* with a central bore, surrounded by a soft iron *pole piece* that is interrupted by a *gap* within the bore. This creates a *nonuniform magnetic field distribution*.

The magnetic field strength and thus, the focal length of the lens can be adjusted by the *coil current*.

The focusing action is based on the inhomogeneous magnetic field distribution: Along the optical axis, the B-field is parallel to the z-axis and **Bell-shaped**:

$$B_z(z) = \frac{B_0}{1+(z/a)^2}$$

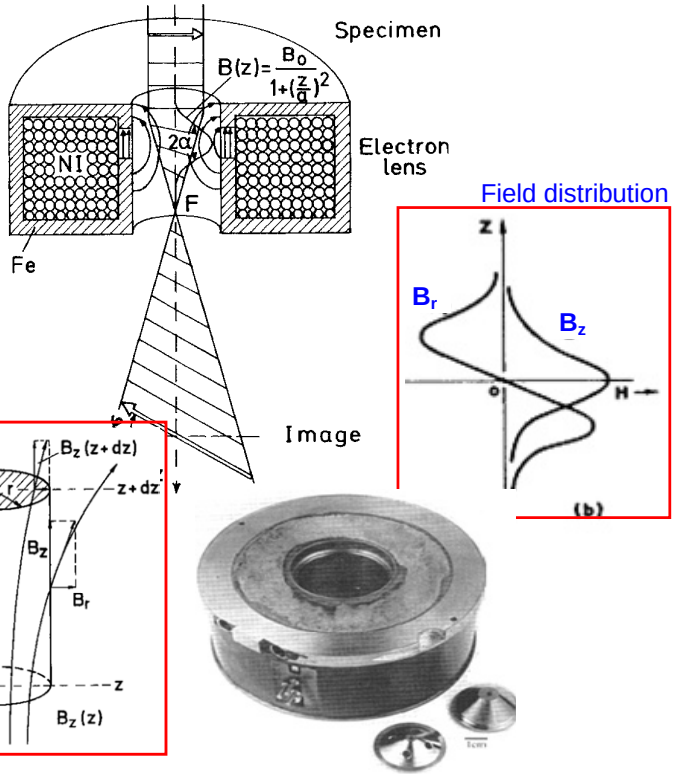

B_0 is the maximal center field and 2*a* the FWHM.

For on-axis electrons, the velocity is parallel to z and therefore, the Lorentz force and deflection is zero.

Away from the optical axis, the radial magnetic field B_r can be deduced from the Gauss law (div B = 0):

$$\pi r^2 B_z(z) - \pi r^2 B_z(z+dz) - 2\pi r B_r dz = 0$$

and $B_z(z+dz) = B_z(z) + (\partial B_z / \partial z)\, dz + \ldots$

$$\Rightarrow \quad B_r \approx \frac{-r}{2}\frac{\partial B_z}{\partial z} = \frac{r \cdot z \cdot B_0}{\left[1+(z/a)^2\right]^2}$$

because *B* is radially symmetric and $B_\varphi = 0$.

As a result of the nonuniform field distribution, the off-axis electrons experience a deflection force directed towards the central axis: It is given by the **Lorentz force**: $\boldsymbol{F_L - ev \times B}$.

Focusing force and motion of the electrons: Using cylindrical coordinates (r,φ,z):

Radial component: $m\ddot{r} = F_r + mr\dot{\varphi}^2$ (1) with the Lorentz force: $F_r = -e \cdot B_z \cdot v_\varphi = -e \cdot B_z \cdot r \cdot \dot{\varphi}$ (2)

Angular component: $d(mr^2\dot{\varphi})/dt = d(e \cdot r^2 B_z/2)/dt$ (3)

$\Rightarrow$ $\dot{\varphi} = \omega_L = e \cdot B_z / 2m$ (4) where ω_L is the Larmor frequency.

z - component: $m \cdot \ddot{z} = F_z \approx 0$ (5) i.e., v_z ~ constant.

Inserting (4) and (2) in (1) yields the *focusing force* of

$$F_r = m\ddot{r} = -\frac{e^2}{2m} \cdot r \cdot B_z^2$$ towards the optical axis: $F_r \sim r$!!

Because this force increases with increasing *r*, the outer electrons are deflected stronger than the inner electrons. This yields a *focusing action* similar as for a optical lenses.

The resulting electron trajectories within a magnetic lens are shown in the graph on the right hand side as a function of the *lens strength ω*:

$\omega = \sqrt{1+k^2}$ where $k^2 = B_0^2 a^2 / 8 m_0 E_{el}$

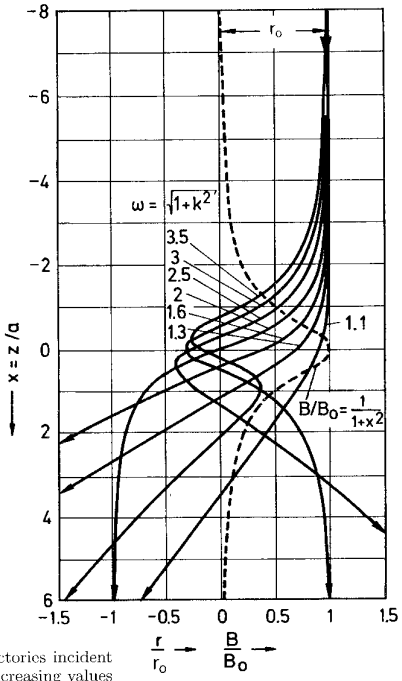

Fig. 2.7. Electron trajectories incident parallel to the axis for increasing values of lens strength $\omega = \sqrt{1+k^2}$ [2.2]

Aberrations of Electron Lenses

The focal points of electrons incident at different distance from the optical axis *r* are not on the same point. Magnetic lenses therefore exhibit rather large lens aberrations:

(i) Spherical Aberration: (Parallel beams are not focused exactly on the same focal point).

» **Broadening of the spot size** r_{sph} in the focal plane. Increases with α: $r_{sph} = C_s \alpha^3$

» **Spherical aberration constant** are typically C_s **~ mm** for TEM lenses, increases with increasing lens strength proportional to the focal length.

Example: For C_s = 3mm => (i) α = 1° (12 mrad) → r_{sph} = 5 nm ; (ii) α = 5° (87 mrad) → r_{sph} = 2 µm

(ii) Chromatic Aberration:

(Slower electrons are bend more strongly than faster electrons)

» Resulting broadening of the spot size (spot radius r_{chr}) is given by: $r_{chr} = C_c \frac{\Delta E}{E_0} \alpha$

» **Chromatic aberration constant** C_c **~ mm**, increases with decreasing lens strength.

Although the energy spread of the primary electrons is typically smaller than 2 eV, the energy spread Δ*E* of the electrons transmitted through the sample is much larger (15 – 25 eV) due to inelastic scattering. Δ*E* increases with increasing sample thickness, i.e., chromatic errors increase.

(ii) Astigmatism: When the pole pieces are not perfectly symmetric and the optical axis not perfectly aligned, the electrons experience a non-uniform not radially symmetric magnetic field: $r_{ast} = \alpha \Delta f$

Scherzer Theorem: Aberrations are ***intrinsic*** for rotational symmetric magnetic lenses and can in principle only be corrected by use of complicated ***multipole lenses***.

3. SEM Resolution

In SEM, the lateral resolution is determined by three main factors:

1. The **diameter of the focused electron beam spot size d_{probe}** on the sample, given by:

$$d_{probe} = \sqrt{d^2_{geometrical} + d^2_{diffraction} + d^2_{abberation}}$$

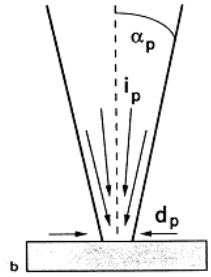

It is determined by the combination of the geometrical spot size d_{geom} as well as the diffraction and abberation broadening d_{diff} and d_{aberr} . These depend on the beam current, aperture angle, lens aberrations, electron energy and wavelength, gun brightness, …..

Note: The **minimal probe size** represents the ***ultimate resolution limit* of SEM** !

2. The **size of the interaction volume** from which secondary electrons and other signal are generated. The interaction volume increases with increasing electron energy and decreasing mass density and Z number of the sample material.

3. **Signal-to-noise noise ratio** (~probe current), **sample contrast, detection mode and efficiency**, type of detector and energy filtering of secondary signals.

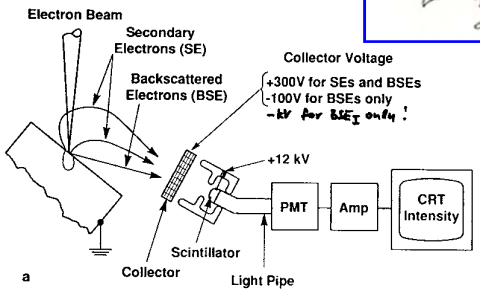

⇒ Points #2 and #3 define the ***practical resolution limit***.

The Geometrical Spot Size and its Relation to the Probe Current

The **SEM lens system** produces a *small electron spot size with diameter d_{probe}* on the sample surface by ***demagnification*** of *the initial beam diameter d_0* at the cross-over within the gun onto the sample using a multiple electron lens system. Thereby, the beam is reduced to a very small size.

Electron gun (thermionic)

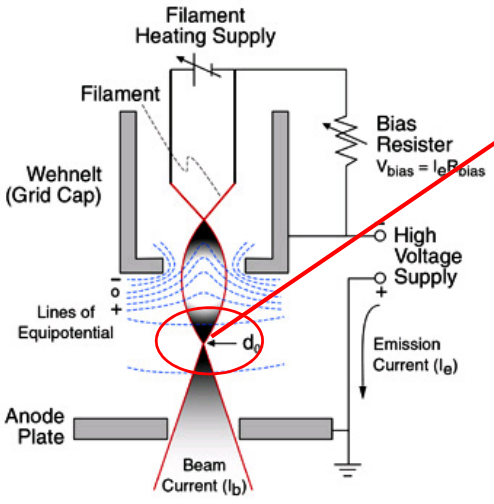

Demagnification Optics

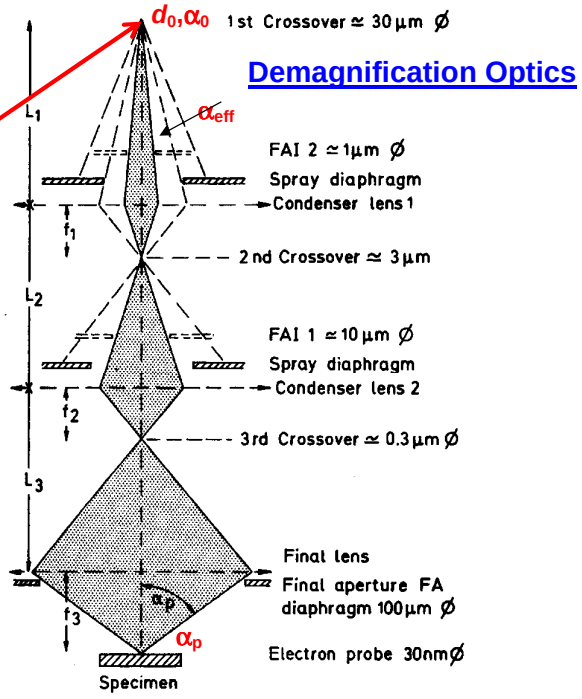

Fig. 2.13. Schematic ray in the electron-optical column of a SEM (FAI = final aperture image)

Demagnification M = $d_{image} / d_{object} << 1$.

For *one lens*: $M = d_{im} / d_{ob} = L_{im} / L_{ob} = \alpha_{out} / \alpha_{in} \approx f / L$

Resulting *geometrical spot size* d_{geom} for a three-lens system:

$$d_{geom} = m_1 \cdot m_2 \cdot m_3 \cdot d_0 = M_{tot} \cdot d_0 \approx f_1\, f_2\, f_3 / (L_1 L_2 L_3) \cdot d_0$$

where d_0 is the initial crossover size of the electron gun.

Thermionic guns: d_0= 50–100 µm, field emitters: d_0~10 nm

⇨**Typical demagnifications**: M = 1/50000… 1/10.

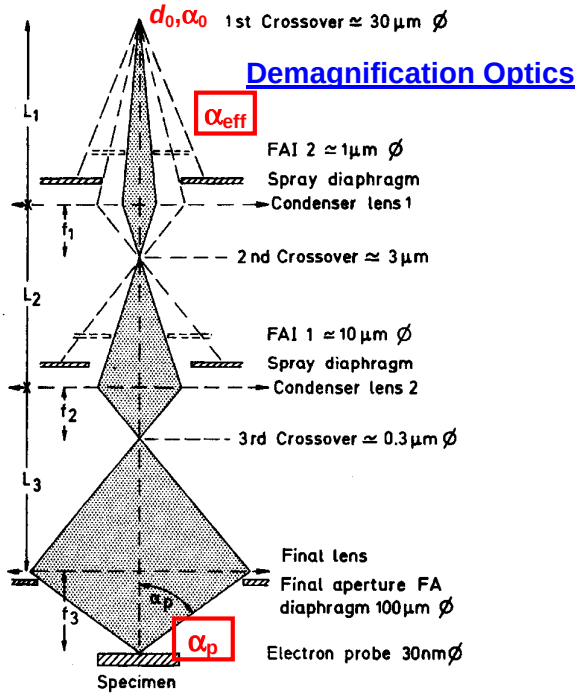

Fig. 2.13. Schematic ray in the electron-optical column of a SEM

Resulting Probe Current I_{probe}

Due to the **final aperture** α_p, actually only ***a small part*** of the initial electron emission cone is projected onto the sample. This strongly reduces the probe current I_{probe}.

The actual *effective emission cone* α_{eff} of electrons emitted from the source focused onto the sample is given by:

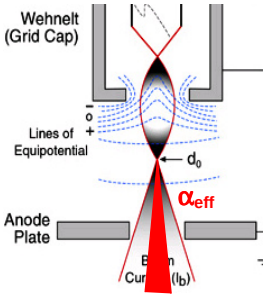

$$\alpha_{eff} = m_1 \cdot m_2 \cdot m_3 \cdot \alpha_p$$

Thus:

$$\alpha_{eff} = M \cdot \alpha_p$$
$$d_{geom} = M \cdot d_0$$

⇨ Reducing the magnification M to achieve a small spot size simultaneously decreases the probe current !

Example: Typical working distance WD = 10 mm (~ f_3) and typical objective diaphragm diameter: 50 … 100 µm.
⇨ Final aperture: α_p = 5 - 10 mrad (0.2°) yields effective source aperture: α_{eff} ~ 10^{-4} mrad !!

Relation between probe current, final aperture and geometrical spot size

As shown above, the final aperture limits the beam current I_p in the final probe spot d_{geom} on the sample because only a reduced cone of emitted electrons with $\alpha_{eff} < \alpha_0$ is focused onto the sample.

The ***total emission current*** I_0 emitted from the electron gun is given by:

$$I_0 = j_0 \, A_0 = (\pi \, \alpha_0^2 \beta) \cdot (\pi d_0^2 / 4)$$ using the gun parameters

d_0 = crossover diameter and *brightness* $\beta = I_e / A_e \Omega = j_0 / \pi \alpha_0^2$

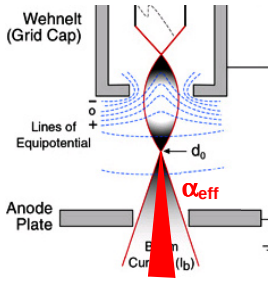

The ***actual probe current*** I_p is then given by:

$$I_p = I_0 \cdot (\alpha_{eff} / \alpha_0)^2 = \pi \, \alpha_0^2 \beta \cdot \pi d_0^2 / 4 \cdot (\alpha_{eff} / \alpha_0)^2 = \tfrac{1}{4} \pi^2 \beta \, d_0^2 \alpha_{eff}^2$$

Using $\alpha_{eff} / \alpha_0 = M$ and $M = d_{geom} / d_0$ yields the relation:

$$I_p = \tfrac{1}{4} \pi^2 \beta \, d_0^2 \cdot M^2 \alpha_p^2 = \tfrac{1}{4} \pi^2 \beta \cdot d_{geom}^2 \cdot \alpha_p^2$$

⇨ Thus, the geometrical spot size and the probe current are interrelated !

$$d_{geom} = \sqrt{4/\beta} \cdot \pi \alpha_p \cdot \sqrt{I_p}$$

Conclusions:

⇨ For a given gun brightness β and final aperture α_p, the reduction of the probe diameter d_{geom} by increasing the demagnification comes at the cost of reducing the beam current I_p !

⇨ An infinitely small geometrical beam spot is achieved only with an infinitesimal small probe current !

For a required probe beam current I_p, the smallest achievable geometrical spot size d_{geom} is given by:

$$d_{geom} = \frac{\sqrt{4/\beta}}{\pi \alpha_p} \cdot \sqrt{I_p} = \sqrt{\frac{4 I_p}{\beta \pi^2}} \cdot \alpha_p^{-1}$$

Influence of the used Electron Guns

From the derived relation: $d_{geom} = \frac{\sqrt{4/\beta}}{\pi\alpha_p} \cdot \sqrt{I_p} = \sqrt{\frac{4I_p}{\beta\pi^2}} \cdot \alpha_p^{-1}$ follows: $I_p = \frac{\pi^2\alpha_p^2}{\sqrt{4}} \cdot \beta \cdot d_{geom}^2$

- ⇨ Thus, for a gun with higher brightness *b*, a much higher beam current can be obtained for a fixed geometrical spot size !
- ⇨ As a result, SEMs equipped with field emission or Schottky LaB_6 guns usually provide a higher microscope performance with higher spatial resolution.

Characteristics of the Three Principal Sources Operating at 100 kV

	Units	Tungsten	LaB_6	Field Emission
Work function, Φ	eV	4.5	2.4	4.5
Richardson's constant	A/m^2K^2	6×10^5	4×10^5	
Operating temperature	K	2700	1700	300
Current density	A/m^2	5×10^4	10^6	10^{10}
Crossover size	µm	50	10	<0.01
Brightness	A/m^2sr	10^9	5×10^{10}	10^{13}
Energy spread	eV	3	1.5	0.3
Emission current stability	%/hr	<1	<1	5
Vacuum	Pa	10^{-2}	10^{-4}	10^{-8}
Lifetime	hr	100	500	>1000

Electron Spot Size due to Diffraction and Aberrations

Neglecting all other factors, the ***ultimate SEM resolution*** is given by the electron spot size d_{probe}, which is larger than the geometrical spot size d_{geom} due to diffraction and lens aberrations.

The **real final spot size d_{probe}** is given by the **root mean square sum of all broadening factors**:

$$d_{probe} = \sqrt{d_{geom}^2 + d_{diff}^2 + d_{sph}^2 + d_{chr}^2}$$

where: (see Chapter 5)

- ❖ d_{geom} is the geometrical spot size, given by: $d_{geom} = (4I_p / \beta\pi^2)^{1/2} / \alpha_p$
- ❖ d_{diff} is the diffraction broadening, given by: $d_{diff} = 0.61\,\lambda / \alpha_p$
- ❖ d_{shp} is the spot broadening due to spherical aberration: $d_{sph} = C_{sph} \cdot \alpha_p^3 / 2$
- ❖ d_{chr} is the spot broadening due to chromatic aberration: $d_{chr} = C_{chr} \cdot \Delta E/E \cdot \alpha_p$

Other lens aberrations are less important.

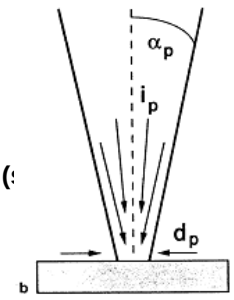

These factors depend on: **Objective aperture α_p, Electron energy *E*, Gun brightness β, Probe current I_p** and Lens properties (aberrations). Inserting the above relations yields:

$$d_{probe}^2 = \left[\frac{4I_p}{\beta\pi^2} + (0.61 \cdot \lambda)^2\right] \frac{1}{\alpha_p^2} + \left(\frac{1}{2} C_{sph}\right)^2 \alpha_p^6 + \left(\frac{\Delta E}{E} C_{chr}\right)^2 \alpha_p^2$$

- ❖ For small α_p, the probe diameter is inversely proportional to α_p , *i.e.*, $d_{probe} \sim 1 / \alpha_p$
- ❖ For large α_p, the probe diameter increases proportional to α_p^3, *i.e.*, $d_{probe} \sim \alpha_p^3$.

⇨ Thus, for a given value of the probe current I_p, gun brightness β and aberration constants $C_{shp,chf}$, there exists a certain ***optimum aperture $\alpha_{p,opt}$*** at which the ***spot size d_{probe} is minimized***.

(1) Dependence of the Spot Size d_{Probe} on Aperture Angle α_p

Thermionic gun: **Plots: d_{probe} as a function of α_p**

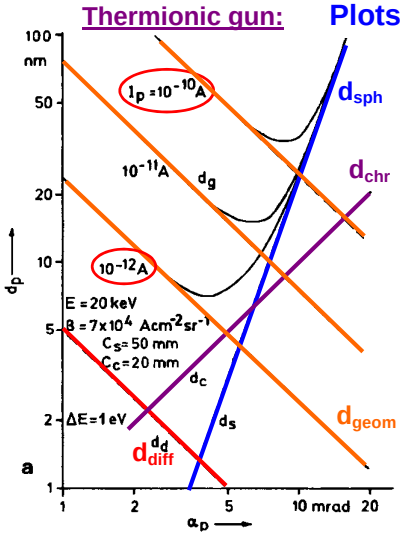

FE gun & in-lens

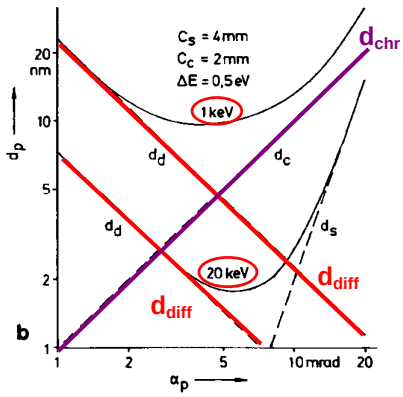

$$d_{probe}^2 = \left[\frac{4I_p}{\beta\pi^2} + (0.61\cdot\lambda)^2\right]\frac{1}{\alpha_p^2} + \left(\frac{1}{2}C_{sph}\right)^2\alpha_p^6 + \left(\frac{\Delta E}{E}C_{chr}\right)^2\alpha_p^2$$

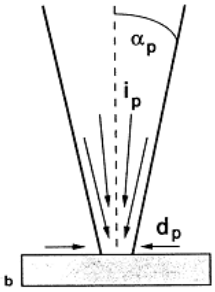

Fig. 2.14. Examples of electron-probe diameters d_p as a function of electron-probe aperture α_p for (**a**) different values of constant electron-probe current I_p using a thermionic cathode and (**b**) for 1 and 20 keV using the in-lens mode and a Schottky or field-emission gun

Cases:

(a) α_p and I_p small: d_p is diffraction limited, *i.e.*: $d_p \sim 1/\alpha_p$

(b) α_p small + I_p large: d_p is limited by current I_p (d_{geom}): $d_p \sim 1/\alpha_p$

(c) α_p large: d_p is limited by spherical aberration: $d_p \sim \alpha_p^3$

(d) α_p intermediate: d_p is limited by chromatic aberration: $d_p \sim \alpha_p$

(2) Dependence of d_{probe} on Beam Current I_p

$$d_{probe}^2 = \left[\frac{4I_p}{\beta\pi^2} + 0.38\lambda^2\right]\frac{1}{\alpha_p^2} + \left(\frac{C_{sph}}{2}\right)^2\alpha_p^6 + \left(\frac{\Delta E}{E}C_{chr}\right)^2\alpha_p^2$$

Thus:

$$d_{probe} = \frac{2}{\beta\pi\alpha_p}\sqrt{\frac{I_p}{\beta}} + Const$$

➢ Smaller spot sizes d_p are obtained for small beam currents I_p and brighter electron guns (FE, LaB_6 - large β) !

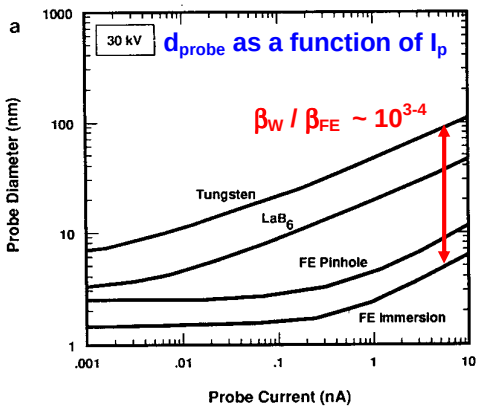

Beam Spot Size

Thermionic gun

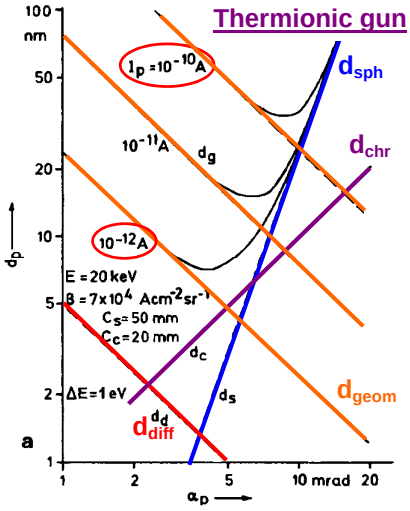

Figure 2.24. Relationship between probe diameter d_p and probe current i_p calculated for tungsten hairpin, LaB_6, and field emission (FE) sources used with a pinhole lens (C_s = 20 mm, C_c = 10 mm). Curves are also shown for the FE source with an immersion lens (C_s = 2 mm, C_c = 2.5 mm). (a) Normal SEM imaging range at 30 kV. (b) SEM range at 10 kV. (c) Low-

FE gun & in-lens

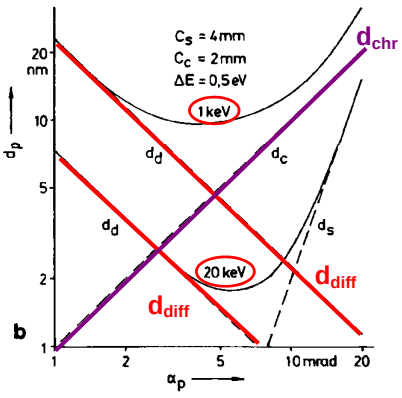

Smaller spot sizes d_p for high brightness field emitter or LaB_6 **electron guns !**

(3) Dependence of d_{probe} on Beam Energy ($\lambda = h/\sqrt{2mE}$)

$$d_{probe}^2 = \left[\frac{4I_p}{\beta\pi^2} + 0.38\lambda^2\right]\frac{1}{\alpha_p^2} + \left(\frac{C_{sph}}{2}\right)^2\alpha_p^6 + \left(\frac{\Delta E}{E}C_{chr}\right)^2\alpha_p^2$$

with $\lambda^2 = \frac{h^2}{p^2} = \frac{h^2}{2mE}$

Thus, for constant current I_p and fixed aperture α_p :

$$d_{probe} \sim \sqrt{C_{const} + C_2 1/E}$$

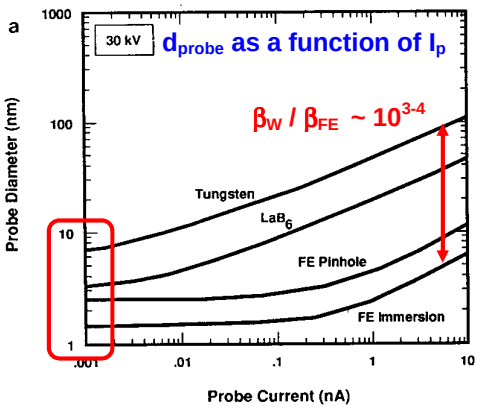

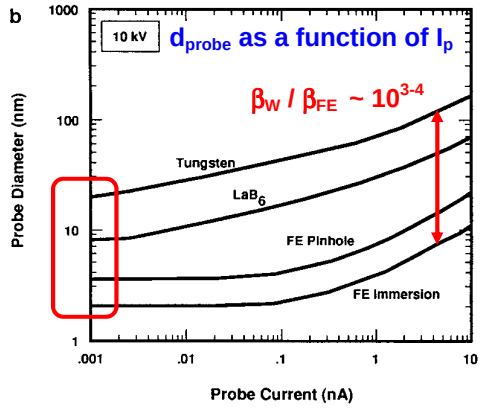

Consequence:

The probe size d_p decreases with increasing electron energy E, at which also the gun brightness β increases !

- **Small α_p:** d_p limited by diffraction: $C_2 = h/\sqrt{2m} \cdot 1/\alpha_p^2$
- **Large α_p:** d_p limited by chromatic aberration: $C_2 = C_{chr}\,\Delta E \cdot \alpha_p^2$
- **Large E**: d_p limited only by I_{probe} and by the spherical aberration constant C_{sph}.

$$d_{probe} = \sqrt{C_{const}} = \sqrt{4I_p/\beta\pi^2\alpha_p^2 + C_{psh}^2/4\alpha_p^6}$$

(4) Optimum Aperture α_p & Minimal Spot Size d_{probe} for a given Probe Current

The probe diameter d_{probe} shows a strong dependence on the final aperture angle α_p described by:

$$d_{probe}^2 = \left[\frac{4I_p}{\beta\pi^2} + 0.38\lambda^2\right]\frac{1}{\alpha_p^2} + \left(\frac{C_{sph}}{2}\right)^2\alpha_p^6 + \left(\frac{\Delta E}{E}C_{chr}\right)^2\alpha_p^2$$

For small α_p, the probe diameter is inversely proportional to α_p , *i.e.*, $d_{probe} \sim 1/\alpha_p$ and for large α_p, the probe diameter increases proportional to α_p^3, *i.e.*, $d_{probe} \sim \alpha_p^3$.

⇨ Thus, for a fixed value of probe current I_p, gun brightness β and aberration constants $C_{shp,chf}$, there exists a certain *optimum aperture* $\alpha_{p,opt}$ at which the *spot size* d_{probe} *is minimized*.

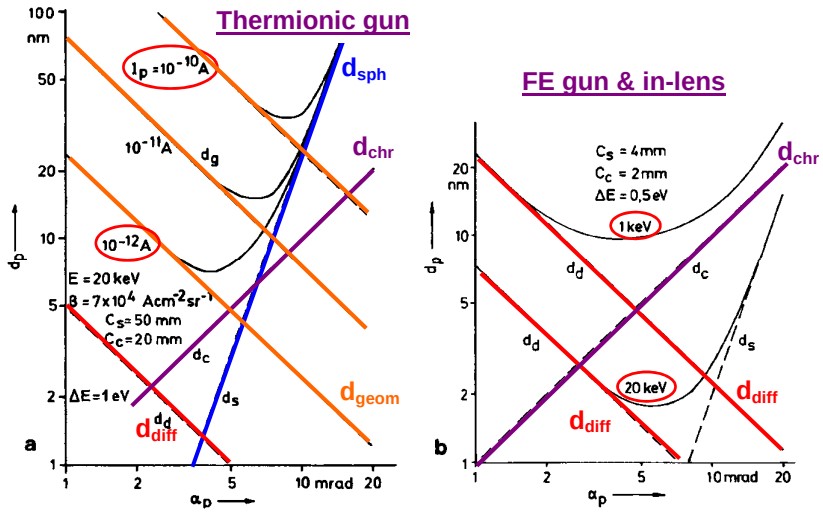

Calculation of the optimum aperture angle α_{opt}:

At high electron energies (>10 kV). the chromatic aberration is smaller than the spherical aberration and can be neglected.

$$d_{probe}^2 \approx \left[\frac{4I_p}{\beta\pi^2} + 0.38\lambda^2\right]\frac{1}{\alpha_p^2} + \left(\frac{C_{sph}}{2}\right)^2 \alpha_p^6$$

Using: $\frac{\partial d_{spot}(\alpha_p)}{\partial \alpha_p} \overset{!}{=} 0$, the optimum aperture angle is obtained as:

This yields: $\alpha_{opt} = \left(\frac{16 \cdot I_p/(3\beta\pi^2)}{C_{sph}^2}\right)^{1/8}$ with corresponding $d_{min} = \left(16 \cdot I_p/(3\beta\pi^2) + 0.38 \cdot \lambda^2\right)^{3/8} \cdot C_{sph}^{1/4}$

Usually, the geometrical spot size d_{geom} is much larger than d_{diff} and therefore, the second term in the brackets can be neglected.

Thus, $d_{min} = \left(16 I_p/3\beta\pi^2\right)^{3/8} C_{sph}^{1/4}$ likewise, for a desired probe diameter the maximum allowed current is $I_{p,max} = \frac{3\pi\beta}{16} \cdot C_{sph}^{-2/3} d_{probe}^{8/3}$

For field emitter guns, $I_{p,max\,c}$ is given by $I_{p,max} = c \cdot d_{probe}^{2/3}$

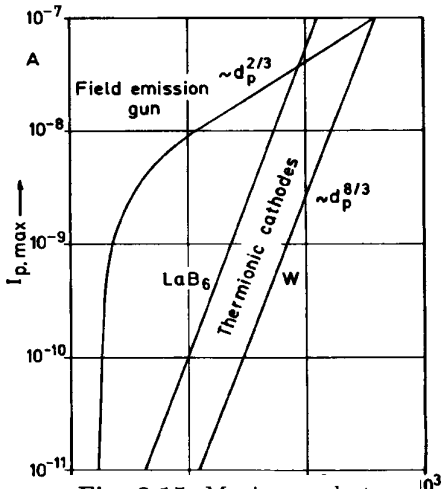

Fig. 2.15. Maximum electron-probe current $I_{p,max}$ plotted against the minimum diameter $d_{p,min}$ for thermionic and field-emission cathodes

Theoretical beam diameter limit:

In the limit of no beam current (I_p = 0), $d_{lim} = (4/3)^{3/8}(0.66 \cdot \lambda)^{3/4} C_{sph}^{1/4}$.

General trends: Smaller probe sizes d_{probe} can be achieved by using:

(i) higher accelerating voltages,
(ii) reduced beam currents,
(iii) electron guns with *higher brightness* β such as field emitter guns,
(iv) *small working distances f,* which reduces the aberration constants.

Other Factors that Influence the Practical Spot Size

Several other factors also degrade the achievable spot size:

- ❖ Alignment of gun, lenses and apertures to minimize beam distortions.
- ❖ Fluctuating electromagnetic stray fields larger than a few mGauss.
- ❖ Filament drift and misalignment.
- ❖ Charging of apertures and the samples due to electron beam induced deposition of insulating hydrocarbon layers on exposed surfaces.
- ❖ Mechanical vibrations and stability.

Thus: $d_{probe,eff} = \sqrt{d_{geom}^2 + d_{diff}^2 + d_{aber}^2 + d_{noise}^2 + d_{etc}^2}$

In All:

- ➢ The smallest spot size is achieved when using: An optimum aperature, high electron energies, small probe currents, small working distances (small focal length), high brightness electron sources. Values as small as few nm can be achieved.
- ➢ The actual spot size $d_{probe,eff}$ is always *larger* than the calculated one.
- ➢ The spot size achievable with field emission guns is about 10 times smaller than for thermionic electron sources for a given probe current.
- ➢ The large interaction volume further decreases the SEM resolution but ultimately, the SEM resolution is limited by the effective probe size !

Depth of Field and Depth of Focus

= Depth *T* over which the image is sharp.

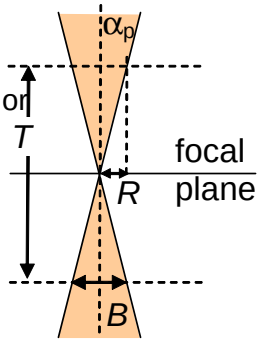

Criterion: Depth over which the broadening *B* introduced by being out of focus is comparable or less than the given lateral resolution *R* or spot size d_{probe}.

Broadening at an offset *T*: $B = T \cdot \tan \alpha_p = R$

Depth of field of SEM: $T = R / \tan \alpha_p$

Due to the very small aperture angles, the depth of field of SEM is two orders of magnitude larger compared to optical microscopes:

Optical Microscope: $T = \lambda / 2\,(NA)^2 = 1.3 \cdot R^2 / \lambda$ [$\delta = 0.61\,\lambda / NA$]

At **low magnification** and **low resolution *R***:

- α_p can be chosen to be very small ~ 1 mrad.
- Therefore, depth of focus *T* is as large as 1 mm !

At **high resolution**:

- α_p ~ 10 mrad but the depth of focus is still above 2 µm !

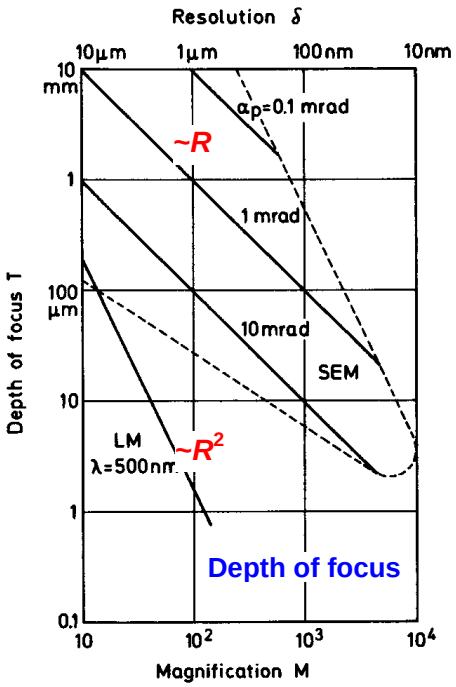

Fig. 2.25. Dependence of the depth of focus *T* on magnification *M* and resolution δ for different electron-probe apertures α_p. *Dotted line*: resolution limit due to Fig. 2.14. For comparison: depth of focus for a light microscope (LM)

Depth of field as a function of SEM operating conditions

Magnification	Image width (μm)[a]	Depth of Field (μm)[b]			
		$\alpha = 2$ mrad	$\alpha = 5$ mrad	$\alpha = 10$ mrad	$\alpha = 30$ mrad
10×	10,000	10,000	4000	2000	667
50×	2,000	2,000	800	400	133
100×	1,000	1,000	400	200	67
500×	200	200	80	40	13
1,000×	100	100	40	20	6.7
10,000×	10	10	4	2	0.67
100,000×	1	1	0.4	0.2	0.067

[a] For a 10-cm CRT display.

[b] $\alpha = 2$ mrad: $R_{AP} = 100\,\mu$m, $D_W = 25$ mm; $\alpha = 5$ mrad: $R_{AP} = 100\,\mu$m, $D_W = 10$ mm; d $= 10$ mrad: $R_{AP} = 200\,\mu$m, $D_W = 10$ mm; $\alpha = 30$ mrad: $R_{AP} = 600\,\mu$m, $D_W = 10$ mm.

Depth of field: Comparison of optical versus electron microscope

Optical Microscope **($T = \lambda / 2\,(NA)^2$: ~ 200nm for HR-OM)**

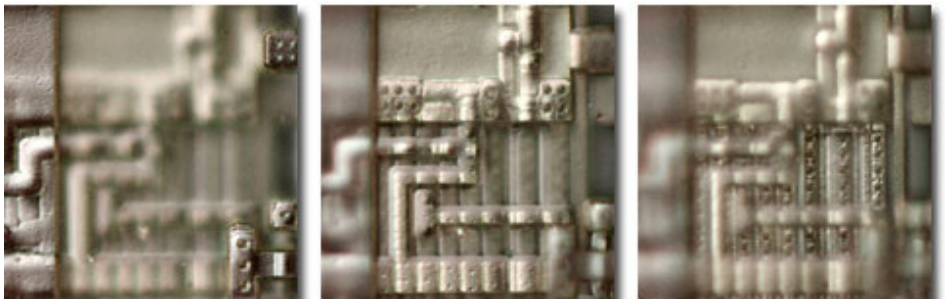

Scanning Electron Microscope **(T ~ 10 -1000 µm)**

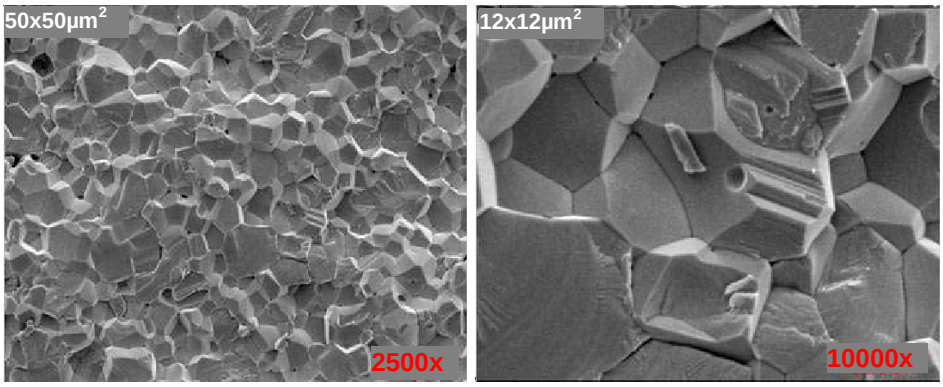

4. SEM Imaging: Backscattered versus Secondary Electron Emission

In SEM/STEM, the **imaging signal** is essentially the **intensity of electrons emitted from the sample** due to the electron bombardment. The emitted electrons consist of two main contributions, namely,

(i) Backscattered Electrons (BSE):

= Primary electrons backscattered from the sample with BSE_I and BSE_{II} components.

(ii) Secondary Electrons (SE):

= Electrons excited and knocked out by the primary electrons entering the sample (SE_I) or by electrons knocked out when BSE leave the sample (SE_{II}) or by secondary processes such as x-ray photons. Practically, all emitted electrons emitted with energy less than 50 eV are considered as SE.

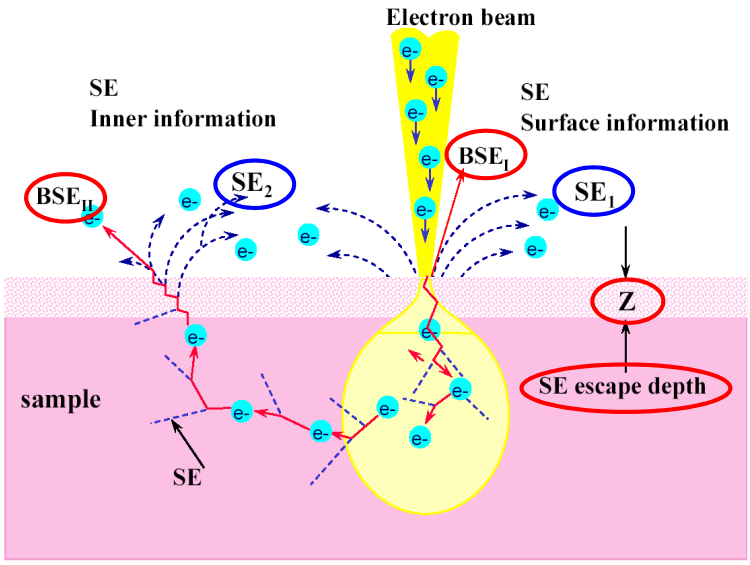

Escape depth Z

Due to the rather **short mean free path λ** of electrons in solids, actually ***only a small fraction*** of the **BSE** and **SE** electrons that are generated within a certain escape depth *Z* underneath the surface can actually escape from the sample and can be collected by an electron detector.

Escape Depth

The **escape depth *Z*** of electrons is about **5 times the mean free path λ**, of electrons in solids.

The **mean free path** is strongly dependent on the electron energy as shown on the right hand side.

Fig. 2.1. Universal curve of electron mean free path: experiment (Rhodin & Gadzuk, 1979; Somorjai, 1981); theory (Penn, 1976).

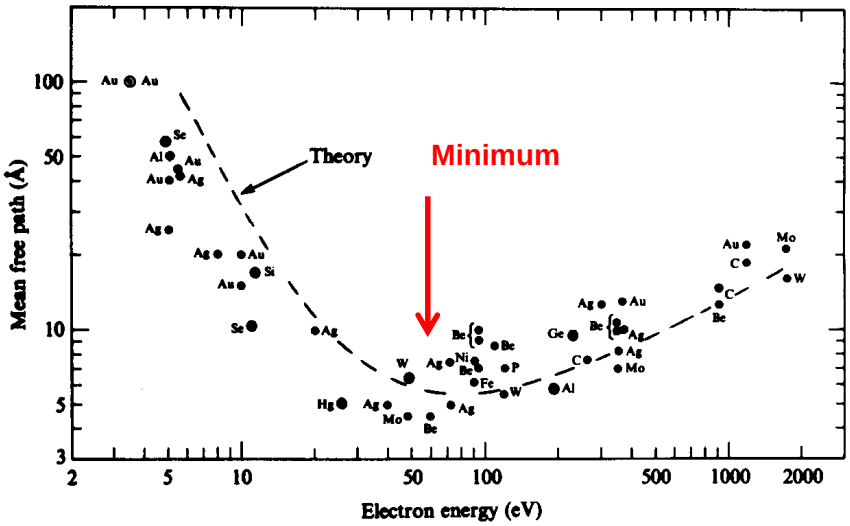

⇒ Essentially all emitted secondary electrons stem from a very thin layer of 5 to 50 nm

Spatial Distribution of Emitted Electrons

Secondary electrons with low kinetic energy: λ ~10 Å for metals, 100 Å for insulators. Z_{escape} ~10nm
Backscattered electrons with higher kinetic energies: λ ~100 Å, i.e., Z_{escape} = 50 nm.

Within each type of emitted electrons (SE or BSE), **different contributions** can be distinguished

Contributions

BSE_I: Localized directly backscattered electrc from single large-angle elastic scatterin near the primary electron spot.
BES_{II}: Delocalized backscattered electrons from multiple small angle scattering events leaving the sample from more remote areas.

SE_I: Localized secondary electrons produced when the primary electrons enter into the sample.
SE_{II}: Delocalized secondary electrons produce when BSE_{II} electrons leave the sample.

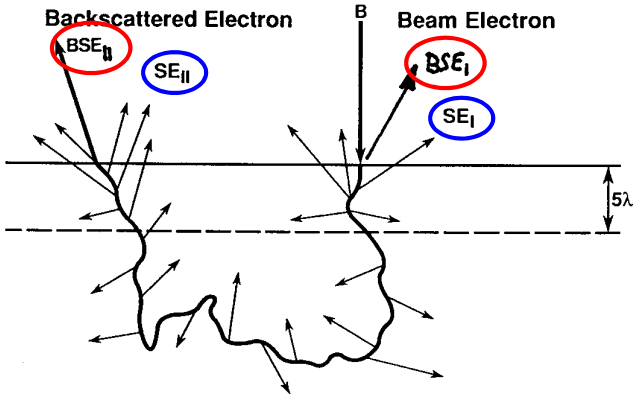

Figure 3.30. Schematic illustration of the origin of two sources of secondary electrons in the sample. Incident beam electrons (B) generate secondary electrons (SE_I) upon entering the sample. Backscattered electrons (BSE) generate secondary electrons (SE_{II}) while leaving the sample. λ is the mean free path for secondary electrons.

SE_{III}: There is an additional ***third contribution SE_{III}*** of ***remotely generated*** secondary electrons produced by electrons scattered from the inner walls of the SEM around the sample.

This creates *a* ***nearly constant background*** of secondary electrons within the SEM chamber.

All high-energy electrons within the sample chamber can produce such remote secondary electrons.

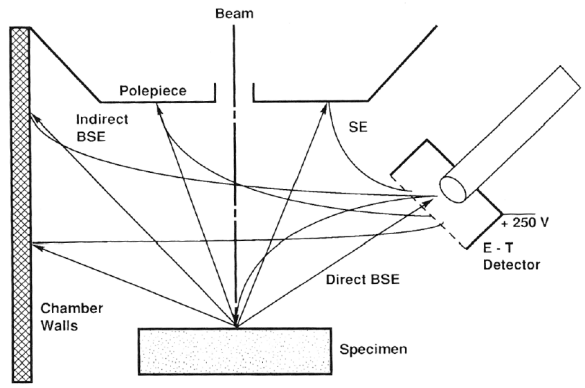

Figure 4.21. Schematic illustration of the indirect collection of backscattered electrons by a positively biased E–T detector. The backscattered electrons strike the polepiece and chamber walls, where they create secondary electrons. These secondaries are collected by the E–T detector with high efficiency. Although nominally a contribution to the secondary signal, they really represent the backscattered-electron signal component.

Example for distribution of electrons:

For Au (or C)	% of Total
• SE_I – beam entering	9%
• SE_{II} – BSE leaving	28%
• SE_{III} – BSE (remote)	61%
• SE_{IV} – Beam at apertures	2%

⇨ **SE_I and BSE_I electrons** are particularly important **for high resolution SEM imaging** because they come from a highly localized spot on the sample surface.

⇨ Due to their low energy of **SE_I** they can be efficiently collected and detected and their shallow escape depth yields high resolution and surface sensitivity.

Lateral Distribution of Backscattered Electrons

The BSEs consists of:

(i) a strongly localized BSE_I peak at primary beam spot.

(ii) a broad outer range of BSE_{II} electrons.

(see below)

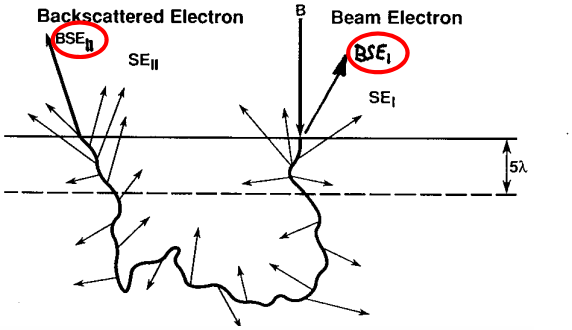

Monte Carlo Simulations:

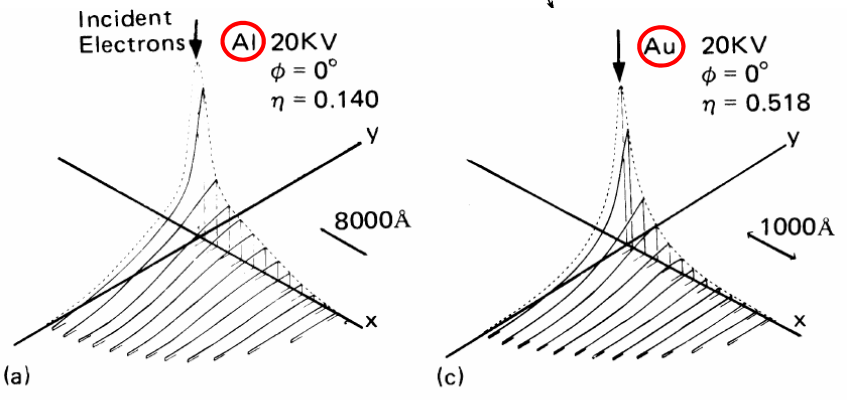

Figure 3.23. Spatial distribution of backscattered electrons from aluminum and gold (E_0 = 20 keV) for 0° tilt and 45° tilt (Murata, 1974).

Lateral range of backscattered electrons

❖ ***Total emission area*** = R_{BS} ~ R_{KO} range.

❖ **But:** Majority of the BSE electrons come from much more localized spot (see prev. Fig).

❖ If one considers the range where x% of the BSE come from, this can be described as:

$$R_{BS}(x\%) = k_{\%} \cdot R_{KO}$$

where $k_{\%}$ is the cut-off proportionality factor:

Table 3.4. Cumulative Radial Backscattering (20 keV)

	$k_{\%}$	a. Distribution Fraction	$k_{\%}$
Element	80%	90%	95%
C	0.502	0.575	0.63
Al	0.419	0.490	0.545
Cu	0.318	0.382	0.439
Ag	0.250	0.310	0.365
Au	0.195	0.248	0.295
	d / R_{KO}	**d / R_{KO}**	**d / R_{KO}**

Both the R_{KO} range as well as proportionality factor $k_{\%}$ decrease with increasing Z number:

⇨ **For higher Z materials, the BSE signal comes from a much smaller spot of the sample !**

Example 90%

- **For pure Al 90% of BSEs are from d/R_{KO} = 0.49**
- **For pure Au 90% of BSEs are from d/R_{KO} = 0.25**

Thus, 90% of the BSE signal for:

- **Au: 0.25 (0.86 μm) = 0.215 μm**
- **Al: 0.49 (4.2 μm) = 2.06 μm**

	Kanaya–Okayama range (μm)			
	Beam energy (keV)			
Target	5	10	20	30
C	0.52	1.7	5.3	10.4
Al	0.41	1.3	4.2	8.2
Cu	0.14	0.46	1.5	2.9
Au	0.085	0.27	0.86	1.7

Lateral Distribution of Secondary Electrons

The secondary electrons consist of two contributions

SE_I (SE_{Beam}) and SE_{II} ($=SE_{BS}$), with and η = backscattering yield.

$$\delta_{tot} = \delta_B + \delta_{BS}\eta$$

⇨ The area of SE_I emission is ~ beam spot size. This yields high resolution SEM images.

⇨ The area of SE_{II} emission is the same as that for BSE_{II} electrons (~R_{KO}).

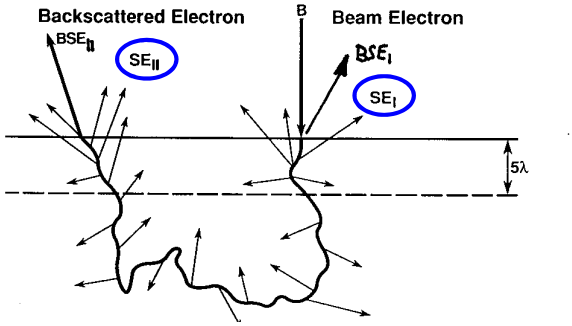

Table 3.8. Ratio of Secondary Electrons Produced by Beam and Backscattered Electrons

	δ_T	η	SE_{II}/SE_I
Carbon	0.05	0.06	0.18
Aluminum	0.1	0.16	0.48
Copper	0.1	0.30	0.9
Gold	0.2	0.50	1.5

Z-dependence:

The ratio of the generation efficiency between δ_{BS} and δ_B is about 3, but the contribution of the BS - SE_{II} is proportional to the BS yield η , which increases with increasing Z.

⇨ Since for high Z materials R_{KO} is smaller, in principle higher lateral resolution can is obtained for higher Z materials.

⇨ However, the total ratio of SE_{II} / SE_I is proportional to the BSE yield η, which increases with increasing Z number. Therefore, for high Z material less SE electrons come from the beam spot on the surface and the SE current is more dominated by the low resolution SE_{II} contribution.

⇨ The increase in lateral resolution for high Z materials is less pronounced than for BSE electrons.

Energy Distribution of Emitted Electrons and Energy Filtering

The **different electron contributions** can be actually ***distinguished*** due to their different ***emission energy***:

Right hand figure:

Typical ***energy spectrum*** of emitted electrons

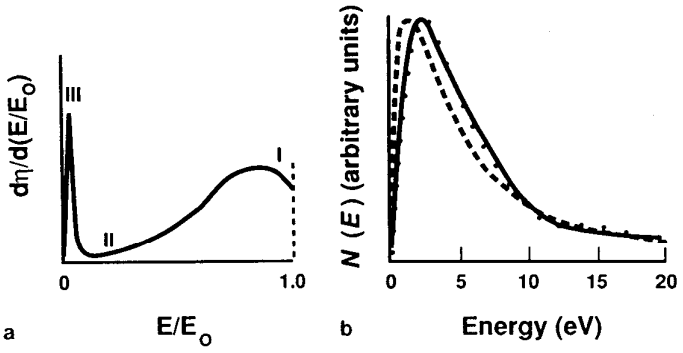

Figure 3.25. (a) Complete energy distribution of electrons emitted from a target, including backscattered electrons (regions I and II) and secondary electrons (region III). Note that the width of region III is exaggerated. (b) Secondary-electron energy distribution as measured (points) and as calculated (lines) with different assumptions on secondary propagation (Koshikawa and Shimizu, 1974).

BSE_I : Electrons with energy close to the primary electrons (low loss electrons).

BSE_{II}: Electrons with intermediate energies.

$SE_{I,II,III}$: Electrons with very low kinetic energies of up to about 20 eV.

⇨ By **energy selective electron detection**, the different contributions can be ***enhanced*** or ***suppressed*****.**

⇨ This is achieved, e.g., by using an **Evenhart-Thornley electron detector.**

Energy Filtering by Electron Detectors

Evenhart-Thornley detector: For high-sensitivity detection of the small electron currents (nA) emitted from the sample, a scintillator-photomultiplier detector is used, in which the emitted electrons are first converted to photons and subsequently amplified by a high gain photomultiplier.

Energy filtering using a collector grid:

(a) **Large positive bias** (attraction of electrons): High collection efficiency for all types of electrons. Thus, the image intensity (current) is high but the spatial resolution low.

(b) **Small negative bias** (repulsion): Suppression of low-energy secondary electrons SE, detection only of BSE.

(c) **Large negative bias** (strong repulsion)**:** Collection of only the directly backscattered BSE_I electrons for high spatial resolution.

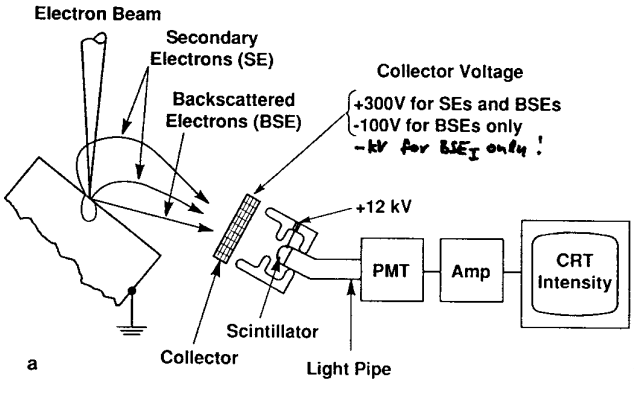

Semiconductor pn/Shottky junction detector:

Impinging electrons create electron hole pairs, causing a current across the reversely biased pn junction.The average number of electron-hole pairs per incident electron is roughly equal to ~ E_0/E_{gap}, where E_{gap} is the semiconductor band gap.
Thus, high energy electrons give a higher signal, therefore, this dector is mainly used for **backscattered electrons**.

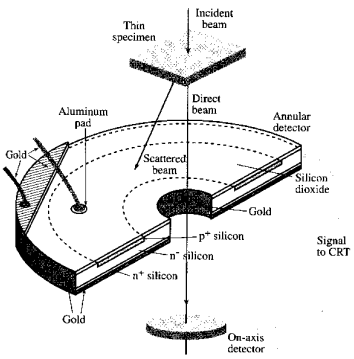

Practical SEM Resolution

(1) Only directly backscattered electrons **BSE_I** and the secondary electrons **SE_I** stem from a highly localized spot around the primary electron beam spot on the surface.

⇨ High lateral resolution can be obtained only from these contributions!

⇨ Under ideal conditions, a resolution nearly equal to the probe size can be achieved.

(2) The high resolution signal is superimposed by a broad background with low resolution.
Thus, the high resolution signal-to-background ratio is often rather small and must be optimized.

⇨ The resolution can be enhanced by discriminating electrons using energy filtering.

(3) Energy dependence: At lower energies, the electron range decreases but the spot size increases.

(4) Z dependence: For high Z materials, the electron range decreases but the contribution from non-local BSEII and SEII increases.

Best resolution:

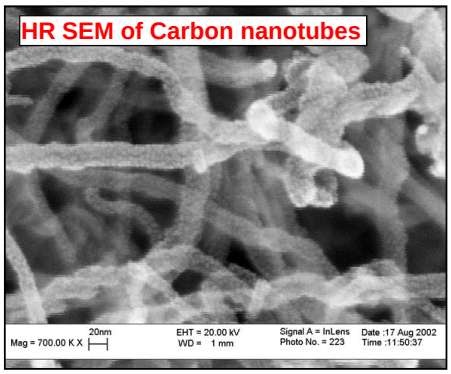

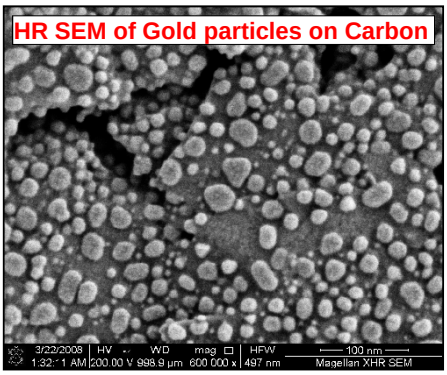

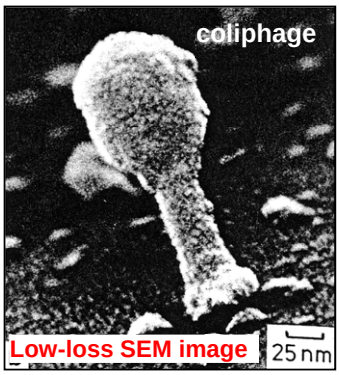

Increased Resolution for Backscattered Electrons by Energy Filtering

Directly backscattered electrons BSE_I with very small energy loss originate from the impingement area of highly focused electron beam: » High resolution imaging possible also with BS electrons.

❖ **Backscattered electrons BSE_{II}**

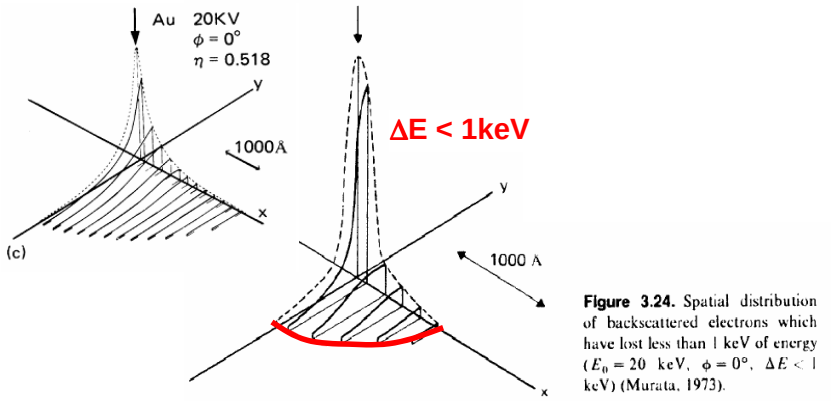

Figure 3.24. Spatial distribution of backscattered electrons which have lost less than 1 keV of energy ($E_0 = 20$ keV, $\phi = 0°$, $\Delta E < 1$ keV) (Murata, 1973).

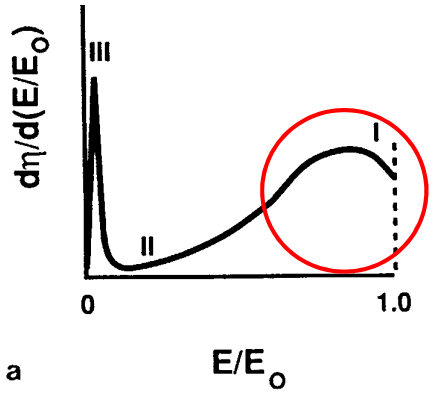

Lateral resolution of BSE signal: $d_{eff} = (d^2_{probe} + d^2_{BSE})^{1/2}$ where d_{BSE} is the emission range for BSE.

» ***d_{BSE}* can be strongly reduced by energy filtering** of the BSE signal by the detector.

» **High-resolution low-loss BSE images** using negatively biased ET or semiconductor detectors.

» But: d_{BSE} is always proportional to R_{KO}: Higher resolution achieved for larger Z and smaller E_{probe}.

5. Contrast in SEM

A. Chemical Contrast - Backscattered Electrons (BS)

The **backscattering yield η** is defined as $\eta = \frac{n_{BS}}{n_0} = \frac{i_{BS}}{i_0}$ n_0 = number of primary electrons

Empirical dependence of BS yield η as a function of atomic number Z (=*Z-contrast*): $\eta = -0.0254 + 0.016Z - 1.86 \times 10^{-4}Z^2 + 8.3 \times 10^{-7}Z^3$

General trends:

- *Increase* of η as a function of atomic number *Z* because Rutherford backscattering is more efficient for heavy atoms.

  The backscattering η yield does *not* show a significant beam energy dependen
- The *contrast C* in backscattered electron images is mainly due to differences in chemical composition in the sample (but also contains some contributions of morphology) and is given by:

$$C = \frac{S_2 - S_1}{S_2} = \frac{\eta_2 - \eta_1}{\eta_2} \qquad \eta_{mix} = \sum_i \eta_i C_i$$

C_i is the concentration of the element *i* within the interaction volume of the sample.

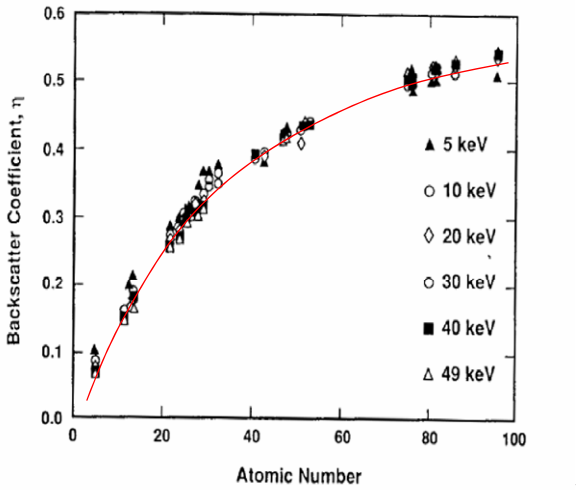

Figure 3.15. Backscattered-electron coefficient as a function of atomic number plotted for a range of beam energies from 5 keV to 49 keV [data of Bishop (1966) and Heinrich (1966a)].

Examples for *Z* contrast in SEM:

Ni-Cd battery element:

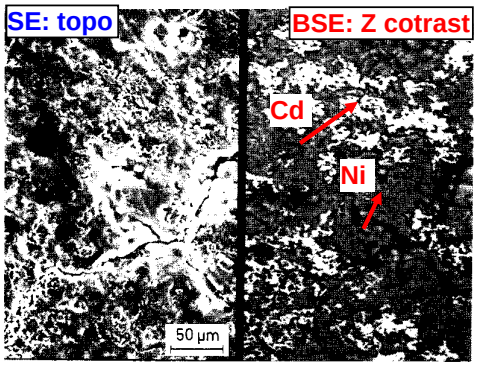

Figure 3-18. Secondary electron and backscattered electron images of the cathode plate of a space satellite battery. The SE image shows only the topography of the surface. The atomic number contrast in the BS image shows that Cadmium (appearing as bright particles) has redeposited across the nickel cathode (darker background).

Al-Ni alloy:

$I_{SC} = I_{probe} - I_{BS}$

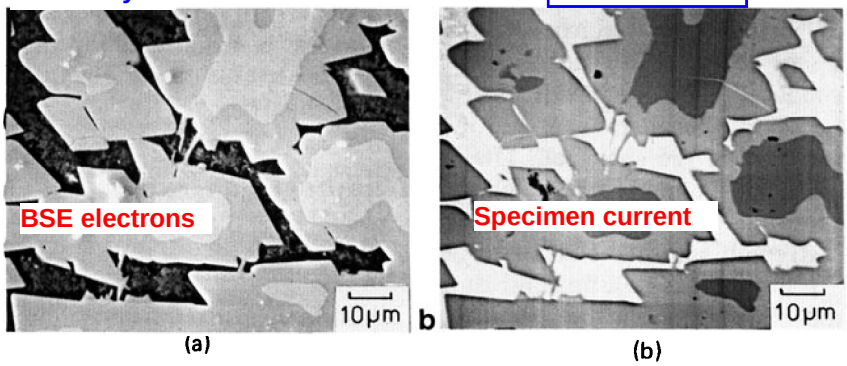

Figure 4.26. (a) Backscattered electron image derived from a reverse-biased Everhart–Thornley detector. (b) Direct specimen current image of the same region as shown in Figure 4.26a. (Note: the faint vertical lines arise from interfering stray signals.) Specimen: Raney nickel alloy (aluminum–nickel); beam energy 20 keV.

B. Topographic Contrast

Topography contrast originates from:

a) Surface tilt contrast due to dependence of SE and BSE yields on local surface tilt relative to electron beam.

b) Shadowing contrast due to orientation of electron collection detector relative to the sample surface.

c) Diffusion contrast due to enhanced SE escape probability at step edges.

Table 3.8. Ratio of Secondary Electrons Produced by Beam and Backscattered Electrons

	δ_T	η	SE_{II}/SE_I
Carbon	0.05	0.06	0.18
Aluminum	0.1	0.16	0.48
Copper	0.1	0.30	0.9
Gold	0.2	0.50	1.5

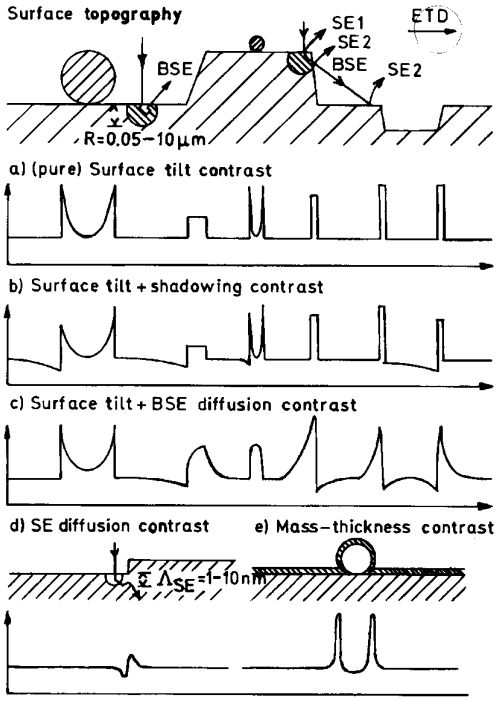

Fig. 6.1. Contributions to topographic contrast demonstrated schematically by surface contours (top) and linescans of SE signals; (**a**) surface tilt contrast, (**b**) shadowing contrast, (**c**) BSE diffusion contrast, (**d**) SE diffusion contrast and (**e**) mass-thickness contrast

Topographic Contrast

Dependence of secondary electron yield as a function of the tilt angle θ between the primary beam and the surface normal is:

$$\delta(\theta) = \delta_0 \sec\theta$$

Origin: For grazing incident primary electrons the trajectories are closer to the surface. Thus, more secondary electrons are generated within the escape depth of the surface.

» Drastic increase of SE electron yield with increasing surface tilt angle.
Very strong topographic contrast secondary electrons as compared to BS electrons.

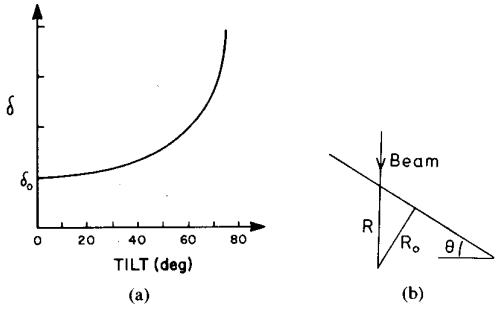

Figure 3.31. (a) Behavior of secondary-electron coefficient δ as a function of specimen tilt θ, following a secant law. (b) Origin of secant law behavior.

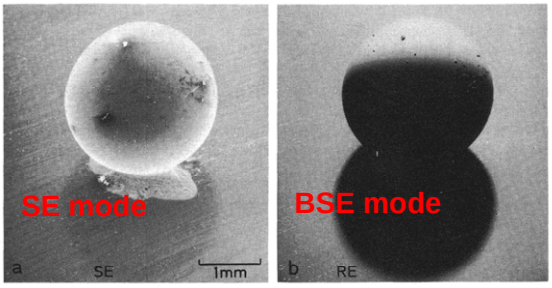

Fig. 6.2. Imaging of a 3 mm steel ball in the (**a**) SE and (**b**) BSE mode with biases of +200 V and –50 V at the collector grid of an Everhart–Thornley detector, respectively, to demonstrate the topographic contrast and the stronger shadow casting in the BSE mode

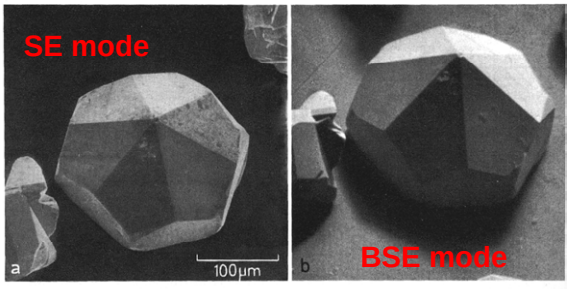

Fig. 6.3. Illustration of surface tilt and shadow contrast with micrographs of $Ge_{38}P_8I_8$ crystals in the (**a**) SE and (**b**) BSE mode

Shadowing Contrast and its Control by the Detector Bias

High-energy BS electrons: Detected only when directly hit the detector » very strong shadowing effects

Secondary SE electrons: Due to positive detector bias, a large fraction of SE is collected by the detector.

SE:

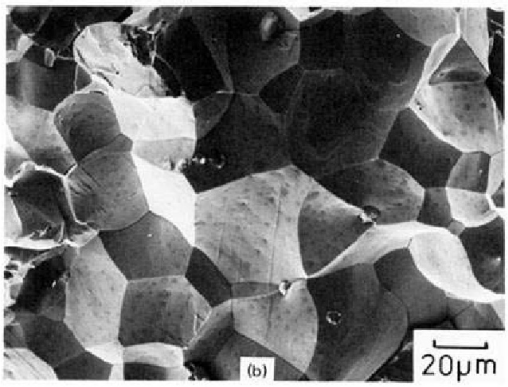

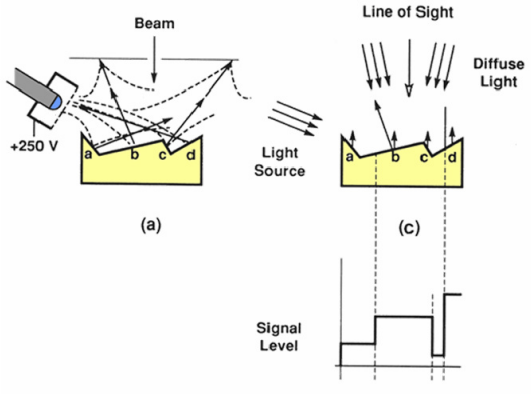

BSE:

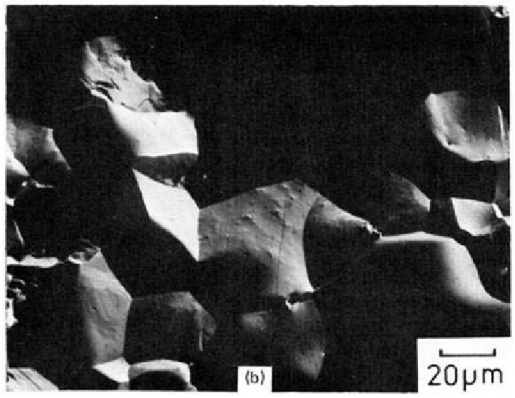

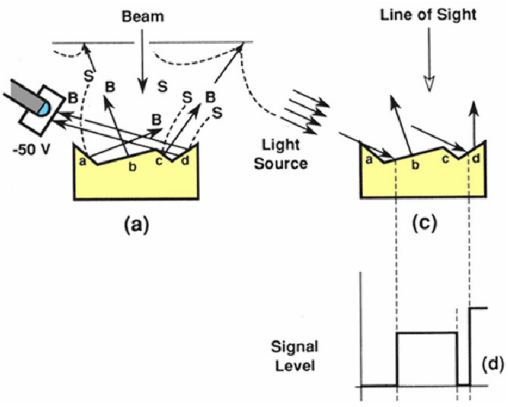

Contrast tuning using different detectors as well as the specimen current signal:

Additional large area solid-state BSE detectors yield a high BSE collection efficiency and a BSE signal with reduced topographic contrast:
This can be used to increase the chemical contrast and to suppress the topography contrast in the BSE images. A **segmented BSE detector** allows an additional contrast tuning.

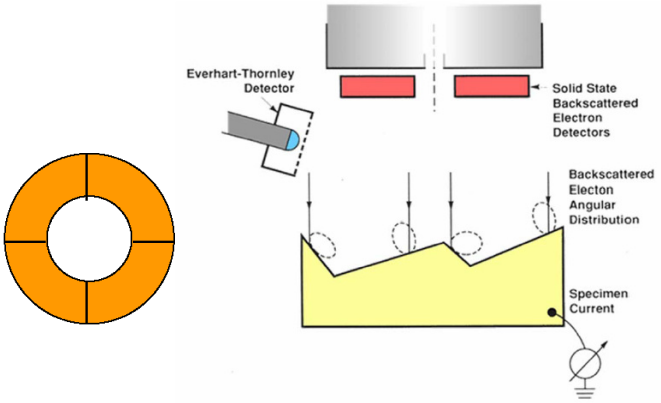

Z-contrast: (A+B) **Topo = (A-B);**

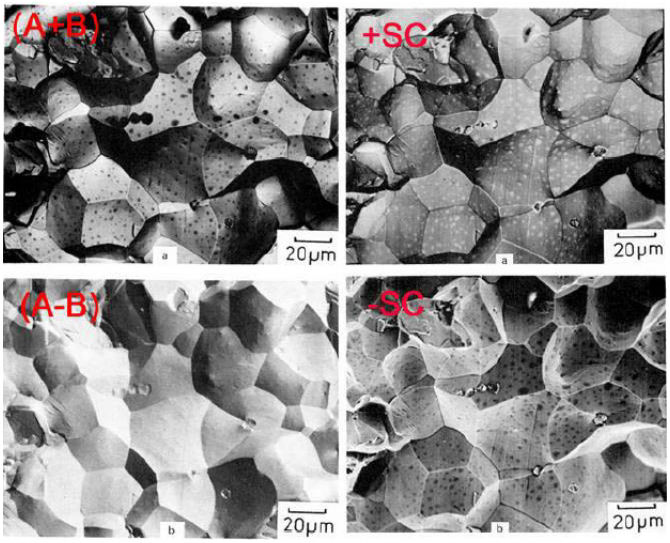

Specimen current: $I_S = I_{probe}\,(1 - \eta_{BS} - \delta_{SE})$:

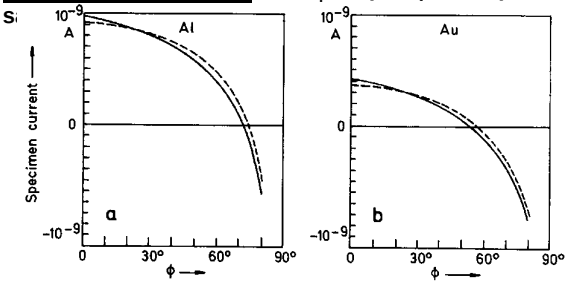

Fig. 6.18. Dependence of the specimen current on the surface tilt angle ϕ for (a) Al and (b) Au (——) experiment, (- - - -) calculated by (6.7)